Journal of Catalysis **203,** 281–291 (2001)
doi:10.1006/jcat.2001.3332, available online at http://www.idealibrary.com on IDEAL®

Differences between MFI- and MEL-Type Zeolites in Paraffin Hydrocracking

Th. L. M. Maesen,*,[1] M. Schenk,† T. J. H. Vlugt,†,[2] and B. Smit†

*Zeolyst International, PQ R&D Center Conshohocken, Pennsylvania 19428-2240; and †Department of Chemical Engineering, University of Amsterdam, Nieuwe Achtergracht 166, 1018 WV Amsterdam, The Netherlands

Received December 11, 2000; revised July 1, 2001; accepted July 1, 2001

A critical evaluation of published paraffin hydroconversion data shows that MEL-type zeolites preferentially hydrocrack paraffins where two methyl groups are separated by a methylene group, whereas MFI-type zeolites prefer paraffins with geminal methyl groups (preferably at the central carbon atom). Due to this difference in hydrocracking pathway, MEL-type zeolites will hydroisomerize a higher percentage of the feed than MFI-type zeolites at low temperature, while the reverse is true at high temperature. The free energies of adsorption calculated by means of configurational bias Monte Carlo (CBMC) molecular simulations are used to explain these differences in selectivity. They show that the MEL- and MFI-type zeolites favor the formation and hydrocracking of the dimethyl paraffins that have a shape commensurate with that of their pores. They indicate that the higher paraffin hydroisomerization selectivity of the MEL-type zeolites can also be explained by their higher selectivity for adsorbing linear rather than branched paraffins at high paraffin loading. At low paraffin loading this difference in adsorption selectivity disappears. Both temperature and loading effects could resolve a disparity in the literature between *n*-decane and *n*-heptane hydroisomerization selectivity data.

Key Words: **molecular simulations; hydrocracking; zeolites; free energies of adsorption.**

INTRODUCTION

Catalysts based on MFI-type zeolites are widely used in many areas of the oil and petrochemical industries, because of their ability to catalyze reactions shape selectively (1). They are used in the catalytic upgrading of fuel oil, because they selectively adsorb and hydrocrack wax-like, long-chain normal paraffins into smaller, shorter-chain products (1–4). Notwithstanding the proven track record of MFI-type zeolites in fuel oil upgrading, a catalyst of comparable activity, but with a higher selectivity for hydroisomerization than for hydrocracking would be desirable as it would yield more valuable fuel oil and less gas. MEL- and MFI-type zeolites are comparable in terms of activity (5–10). This is probably related to the similarity of the framework density and the pore size of these structures (11). Despite these similarities, some studies have suggested that MEL-type zeolites hydroisomerize more paraffins than MFI-type zeolites, at any given paraffin hydroconversion level (5–7). This intrinsic high hydroisomerization selectivity was first postulated based on studies using *n*-decane (n-C_{10}) as a model feed (5), refuted based on studies using *n*-heptane (n-C_7) as a feed (8), and then corroborated by studies using complex feed stocks (6, 7). It is not clear how the differences in structure between MFI- and MEL-type zeolites translate to the differences in catalytic behavior (8).

Both MFI- and MEL-type zeolites have three-dimensional ~0.55-nm channels. The MFI topology consists of intersecting straight and sinusoidal channels, whereas the MEL topology has only straight channels. Consequently, the structure and size of the single MFI-type channel intersection is significantly different from the two distinct MEL-type intersections (Fig. 1) (9, 11).

Before the advent of molecular simulations, relating the differences between the MFI- and MEL-type zeolite structures to differences in shape selectivity was hindered by a lack of microscopic information on the adsorption and diffusion inside these zeolite structures (2, 9). Fortunately, molecular simulations capable of yielding such information on a molecular level have become available (12, 13). However, simulating the adsorption of long-chain or branched paraffins with conventional molecular simulation techniques would require excessive CPU time. Therefore most molecular simulations are energy minimization studies that ignore entropic contributions (14). The configurational bias Monte Carlo (CBMC) technique, a recent development in molecular simulations, circumvents this problem and allows calculation of the Henry coefficients, the free energy of adsorption and the adsorption enthalpy at zero coverage, the diffusion coefficients, and the adsorption isotherms for paraffins in microporous silica structures

[1] Current address: Chevron Research and Technology Co., 100 Chevron Way 10-1412, Richmond, CA 94802. E-mail: tmsn@chevron.com.

[2] Current address: Instituut-Lorenz for Theoretical Physics, P.O. Box 9506, 2300 RA Leiden, The Netherlands.

0021-9517/01 $35.00

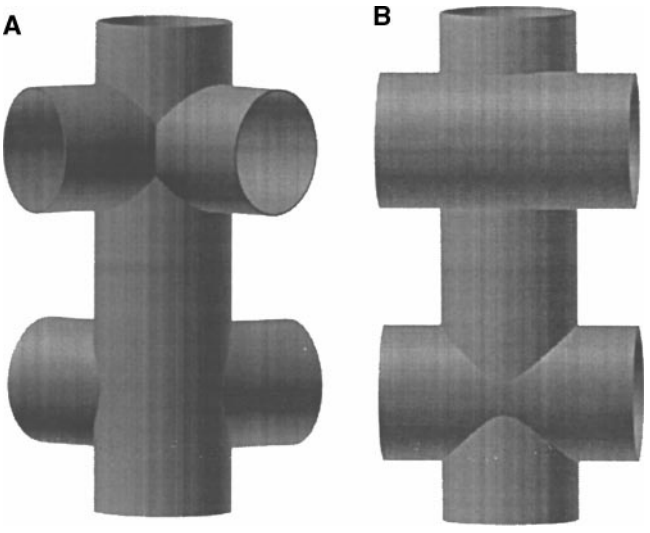

FIG. 1. Sketch of the MFI- (A) and MEL-type (B) channel intersections. The zeolites have a similar pore diameter (0.55 nm) and structure. The principle difference is that MFI contains both straight and sinusoidal channels, while all MEL-type channels are straight. There is only one MFI-type channel intersection. MEL-type channel intersections are either large (top) or small (bottom).

(12, 15–17). The free energy of adsorption quantifies how a zeolite structure alters the gas phase free energy of formation of a hydrocarbon. The more a zeolite structure decreases the free energy of formation for a particular type of paraffin, the more likely it is to form and subsequently hydroisomerize or hydrocrack that paraffin (12).

Here we show how the thermodynamic data obtained by molecular simulations can shed some light on the differences in paraffin hydroconversion between MFI- and MEL-type zeolites. As the thermodynamic adsorption data relate to the shape selective properties that are intrinsic to a zeolite structure, we develop a criterion to identify catalytic data that are unimpaired by mass transport or hydrogenation rate limitations. A subsequent scrutiny of the published *n*-C_7 (8, 18) and *n*-C_{10} (5, 19–23) hydroconversion data using this criterion shows intrinsic differences in paraffin hydroconversion between MFI- and MEL-type zeolites. Simulated C_{10} adsorption data are then used to explain the observed differences in the hydroconversion of *n*-C_{10} and of complex feedstocks and the absence of such differences in a publication (8) on the hydroconversion of *n*-C_7.

MOLECULAR SIMULATION METHODS

In conventional simulations, Monte Carlo moves insert a molecule in a zeolite in a random position. For long-chain hydrocarbons almost always one of the atoms of such a molecule will have an overlap with the zeolite framework. As a consequence, such moves have a very low acceptance rate. Therefore, the application of the conventional Monte Carlo technique is limited to the adsorption of very small probe molecules. In the CBMC scheme the molecules are grown atom by atom in such a way that the empty channels inside the zeolite are found. The bias introduced by this growing scheme is removed by adjusting the acceptance rules (24).

The CBMC simulations model uses single interaction centers (united atoms) to represent the CH_3, CH_2, and CH groups in the linear and branched paraffins. The bonded interactions include bond-bending and torsion potentials. Dispersive interactions with the oxygen atoms of the silica structure are assumed to dominate the silica–paraffin interactions. The zeolite is modeled as a rigid crystal (25), consisting exclusively of SiO_2, so as to make the calculation of paraffin–zeolite interactions efficient. This allows the use of special interpolation techniques (26, 27) to obtain the correct paraffin conformation at any given temperature. More details about the simulation method and the force fields are described elsewhere (24).

The sizes of the molecules and the energy parameters have been fitted to the adsorption enthalpies and the Henry coefficients of linear and mono-branched paraffins in aluminum-free MFI-type silicas (24). The resultant force field reproduces the Henry coefficients, the changes in the free energy of formation (i.e., the free energy of adsorption), the adsorption enthalpies, and isotherms for linear and mono-branched paraffins. The same force field also reproduces these parameters for microporous silica topologies other than the MFI-type remarkably well (28).

The simulations consist of three different trial moves:

1) Displacement of a chain: a chain is selected at random and given a random displacement. The maximum displacement was taken such that 50% of the moves were accepted.

2) Rotation of a chain: a chain is selected at random and given a random rotation around the center of mass. The maximum rotation angle was selected such that 50% of the moves were accepted.

3) Complete regrowth of the chain: a chain is selected at random and is completely regrown at a randomly selected position. During this step data is collected from which the Henry coefficient is determined.

The calculation of an adsorption isotherm of a mixture of alkanes requires a simulation in the grand-canonical ensemble (24). Such a simulation employs the same initial two steps as one in the NVT ensemble, but diverges at the third step:

3) Partial regrowth of the chain: a randomly selected part of a randomly selected alkane is regrown.

4) Exchange with the reservoir: an alkane is randomly added or removed from the microporous silica structure.

5) Identity change: an attempt is made to change the isomer type of a randomly selected molecule.

The relative probabilities for attempting these moves in an NVT simulation were such that 10% of the total number

of moves was a displacement, 10% a rotation, and 80% a regrowth of the entire molecule. A simulation consists of 5×10^6 Monte Carlo steps. In the grand-canonical simulations the probabilities were 15% displacement, 15% rotation, 15% partial regrowth, 50% exchange, and 5% identity change. A typical simulation requires some 10^7 Monte Carlo steps. The calculation of the change in the free energy of formation, the Henry coefficient and the adsorption enthalpy at zero coverage requires two simulations in the NVT ensemble; one simulation of a paraffin inside an MFI- or MEL-type silica and another simulation in the ideal gas situation (24).

In each simulation the Rosenbluth factor is calculated in the molecular sieve, W_{sieve}, and in the ideal gas phase W_{gas}. The free energy of adsorption (ΔG_{ads} (J/mol)) is the difference between the free energy of formation of a molecule in the molecular sieve ($\Delta G^{\text{f}}_{\text{sieve}}$ (J/mol)) and the free energy of formation of one in the ideal gas phase ($\Delta G^{\text{f}}_{\text{gas}}$ (J/mol)). At the limit of very low adsorbate loading and pressure, the Helmholtz and Gibbs free energies converge, so that they follow from the ratio of the Rosenbluth factors (27, 29):

$$\Delta G_{\text{ads}} = \Delta G^{\text{f}}_{\text{sieve}} - \Delta G^{\text{f}}_{\text{gas}} = -R \cdot T \cdot \ln(W_{\text{sieve}}/W_{\text{gas}}). \quad [1]$$

In this formula R is the gas constant (8.3144 J/mol K) and T (K) the absolute temperature.

According to this formalism, the relationship between the free energy of adsorption and the Henry coefficient, K_{H} (mol/kg Pa) is (27, 29)

$$\Delta G_{\text{ads}} = -R \cdot T \cdot \ln(K_{\text{H}} \cdot D \cdot R \cdot T). \quad [2]$$

In this formula D is the framework density (1.79×10^3 kg/m^3 for MFI-type silicas and 1.77×10^3 kg/m^3 for MEL-type silicas (11)).

RESULTS AND DISCUSSION

C_7 hydroconversion mechanism. The hydroconversion of n-C_7 on MFI- (18) and MEL-type (8) zeolites can be described as a series of consecutive reactions (30). First, n-C_7 hydroisomerizes into iso-heptane (i-C_7), then into dibranched heptanes (henceforth referred to as ii-C_7), which subsequently hydrocrack into iso-butane (i-C_4) and propane (C_3) (28, 30):

$$n\text{-}C_7 \rightleftarrows i\text{-}C_7 \rightleftarrows ii\text{-}C_7 \rightarrow i\text{-}C_4 + C_3. \quad [3]$$

The equilibration between the different C_7 isomers occurs inside the MFI- and MEL-type pores. It is not necessarily observed directly in the product distribution due to the interference of diffusion and—occasionally—of premature hydrocracking.

Diffusion affects the product slate by selectively trapping the slowly diffusing i-C_7 (13, 31, 32) and the even more slowly diffusing ii-C_7 with proximate methyl groups (12, 33–36) inside the MFI- and MEL-type pores. The more slowly a C_7 isomer diffuses, the greater the chance that it is hydroisomerized into ii-C_7 with either geminal methyl groups or with methyl groups separated by one methylene (–CH_2–) group (quasi-vicinal methyl groups). These are subsequently hydrocracked into a fast-diffusing i-C_4/C_3 product pair.

Premature hydrocracking affects the product slate when a C_7 isomer is hydrocracked before it has hydroisomerized into geminal or quasi-vicinal ii-C_7. It yields an n-C_4/C_3 instead of an i-C_4/C_3 product pair (28, 37–39). It occurs when there are multiple transformations at acid sites inside pores that significantly limit sorbate mobility (14, 28, 38, 40). This happens when the hydrogenation function is insufficiently active as compared to the acid function (38, 41–43) or when the mass transport between the hydrogenating sites and the acid sites is the rate-limiting step (18, 38, 41, 43).

C_{10} hydroconversion mechanism. It has been shown that n-C_7 and n-C_{10} share essentially the same hydroconversion mechanism (37, 39, 44, 45, 46). The only difference between n-C_7 and n-C_{10} is that the latter can hydroisomerize into a tribranched "iii-C_{10}" isomer with both geminal and quasi-vicinal methyl groups (i.e., with methyl groups on α,α,γ positions) (39, 44–48) before hydrocracking, whereas the former is too short to form the equivalent iii-C_7 hydrocracking precursor. This difference is irrelevant when studying MFI- and MEL-type frameworks, because the shape-selective constraints imposed by these frameworks impede the formation of the transition state required for such iii-C_{10} isomers (5, 12, 49). Thus, for the purpose of this paper, the hydroconversion of n-C_{10} may be regarded as completely analogous to that of n-C_7: n-C_{10} hydroisomerizes into iso-decane (i-C_{10}) and dibranched decanes (henceforth referred to as ii-C_{10}), and subsequently ii-C_{10} hydrocracks to give four product pairs—a monomethyl paraffin i-C_x and a linear paraffin n-$C_{(10-x)}$ (x an integer, $4 \leq x \leq 7$) (50):

$$n\text{-}C_{10} \rightleftarrows i\text{-}C_{10} \rightleftarrows ii\text{-}C_{10} \rightarrow i\text{-}C_x + n\text{-}C_{(10-x)}. \quad [4]$$

As with n-C_7 hydroconversion, the more the n-C_{10} hydroconversion rate is determined by the rate of the acid-catalyzed reactions, rather than by the mass transport or the hydrogenation rate, the higher the proportion of branched paraffins in the product slate (10).

In view of the striking similarity of the n-C_7 and the n-C_{10} hydroconversion mechanism it is intriguing why MEL-type zeolites reportedly have a higher n-C_{10} hydroisomerization selectivity than MFI-type zeolites (5), but not a higher n-C_7 hydroisomerization selectivity (8). This study attempts to resolve this puzzle. To some degree resolution can be obtained by scrutinizing the published n-C_{10} hydroconversion data.

TABLE 1

The Crystal Size, the Framework Aluminum Density (N(Al) in Atoms per Unit Cell), and Zeolite Type of Catalysts Operated at a Partial Hydrogen (p H_2 (kPa)), Hydrocarbon Pressure (p n-C_{10} (kPa)), Molar Hydrogen-to-Hydrocarbon Ratio (H_2/n-C_{10} (mol/mol)) Require a Certain Temperature for 50% n-C_{10} Hydroconversion ($T_{50\%}$ (K))

Zeolite type:	MFI	MFI	MFI	MFI	MFI		MEL
Crystal size (μm)	np[a]	15	6	4 by 6	0.1 by 0.5		4 by 6
N(Al) (at/u.c.)	5.2	2.5	1.6	3	1.6		3
p H_2 (kPa)	100	101	350	100	2000		100
p n-C_{10} (kPa)	1.4	0.7	0.9	1.5	20		1.5
H_2/n-C_{10} (mol/mol)	71	151	389	65	100		65
$T_{50\%}$ (K)[b]	440	440	440	400	520		430
% n-C_{10} hydroconversion	4	7[b]	12[b]	10[b]	46	93[b]	49[b]
% C_{10} hydrocracked	3–4[b]	5	7	5	7	50	5
%i-C_5	25[b]	31	42[b]	44	np[a]	49[b]	50[b]
$^1/_5\sum_{x=4}^{7}$% i-C_x	19[b]	23	34[b]	35	np[a]	47[b]	41[b]
mol C_7 hydrocracked/100 mol C_{10} hydrocracked	0	1	3[b]	2	4[b]	np[a]	1[b]
Reference	(20)	(21)	(22)	(5)	(19)	(19)	(5)

Note. At a % n-C_{10} hydroconversion the catalysts hydrocrack a certain percentage of the feed (% C_{10} hydrocracked), and they yield a percentage branched isomers in the secondary hydrocracking product slate ($^1/_5 \cdot \sum_{x=4}^{7}$% i-C_x, with % i-C_x the percentage of i-C_x in each of the the four C_x fractions, and divided by five to account for the intrinsically linear C_3 fraction) and in the C_5 fraction (% i-C_5). As only heptane (C_7) isomers are liable to secondary hydrocracking (21, 39, 51) the extent of secondary hydrocracking is referred to as "mol C_7 hydrocracked/100 mol C_{10} hydrocracked." It was calculated by halving the difference between the molar C_3 and C_7 yield per 100 mol of hydrocracked decane (C_{10}). The n-C_{10} hydroconversion catalysts that we discuss were loaded with either 0.5 (19, 20) or 1.0 wt% Pt (5, 21, 22, 23). For comparison, the n-C_7 hydroconversion catalysts were loaded with 0.4 wt% Pt (8).

[a] np, not published.

[b] Estimated graphically.

Criteria for identifying mass transport or hydrogenation rate limitations. The intrinsic shape-selective properties of zeolites can be compared only when the acid-catalyzed reactions inside the zeolite pores determines the overall paraffin hydroconversion rate (10), i.e., in the absence of premature hydrocracking due to mass transfer or hydrogenation rate limitations. In principle, it should be straightforward to identify MFI- and MEL-type zeolite catalysts in which the acid catalysis step determines the paraffin hydroconversion rate, for these catalysts characteristically (i) yield a primary (i.e., before secondary reactions) hydrocracking product slate consisting of equal amounts of linear and branched paraffins (Eq. [4]), (ii) yield a primary C_7 fraction consisting exclusively of i-C_7 (Eq. [4]), (iii) yield a primary C_5 fraction consisting of equal amounts of n-C_5 and i-C_5 (Eq. [4]), and (iv) have a low (primary and secondary) hydrocracking selectivity (10, 41–43). In practice, consecutive hydrocracking and hydroisomerization yield a secondary product slate interfering with a straightforward identification (19). The primary i-C_7 isomers are particularly prone to consecutive reactions, because they are the most reactive (37, 39, 51) and because they will stay adsorbed longer than the other primary hydrocracking products will (52). By contrast, the C_5 isomers are relatively unreactive (37, 39, 51) and are short enough to desorb rapidly (and stay desorbed) due to competitive adsorption with longer molecules (52). Thus, of the four criteria a C_5 fraction consisting of equal amounts of n-C_5 and i-C_5 (iii) and a low hydrocracking selectivity (iv) are the least affected by secondary reactions, and therefore are the most straightforward criteria for identifying MFI- and MEL-type zeolite catalysts in which the acid catalysis step determines the paraffin hydroconversion rate.

Mass transport or hydrogenation rate limitations. An examination of the published n-C_{10} hydroconversion data (Table 1 (5, 19–22)) shows that only one paper (19) discusses an MFI-type zeolite catalyst that yields a secondary hydrocracking product slate with a C_5 fraction consisting of close to 50% i-C_5. At 46% n-C_{10} hydroconversion, this catalyst loses only 7% of the C_{10} feed through hydrocracking (%C_{10} hydrocracked, Table 1), whereas at that same conversion level the other catalysts lose more than 35% of the C_{10} feed (5, 20–22). This low primary hydrocracking selectivity, the small amount of secondary hydrocracking (mol C_7 hydrocracked/100 mol C_{10} hydrocracked) at a high % n-C_{10} hydroconversion, and the high percentage of branched paraffins in the secondary hydrocracking product slate ($1/5\sum_{x=4}^{7}$ % i-C_x) (Table 1, also explains formula) all indicate that this particular MFI-type zeolite catalyst

exhibits minimal mass transport and hydrogenation rate limitations (10, 41–43). The other tabulated MFI-type zeolite catalysts yield significantly less than 50% i-C_5 and have a high hydrocracking selectivity (Table 1). This is characteristic for hydroconversion dominated by the mass transport or hydrogenation rate and not by the acid-catalyzed reactions. They employ crystals that are too large, have too high an acid site density, or are operated at such a low hydrogen partial pressure (41, 50) that the C_{10} mass transport rate between the acid sites inside the crystals and the (de-) hydrogenation sites at the crystal's surface (10) is rate limiting (38, 43). Remarkably, also very small MFI-type zeolite crystals cluttered with amorphous debris from a prematurely aborted zeolite synthesis exhibit the high hydrocracking selectivity (4–5% C_{10} hydrocracked at 8–9% conversion (23), cf. Table 1) that is characteristic for mass transport or hydrogenation rate limitations. The preponderance of studies on Pt-loaded MFI-type zeolite catalysts in which the n-C_{10} hydroconversion rate was not dominated by the acid catalyzed reactions could explain why the premature i-C_{10} hydrocracking used to be considered so important (5, 10, 19, 22).

In addition to an MFI-type zeolite catalyst, there is a MEL-type zeolite catalyst for which n-C_{10} hydroconversion data have been published that meets the percentage i-C_5 criterion and that shows a low hydrocracking selectivity (Table 1), indicating that intracrystalline acid catalyzed reactions determine the n-C_{10} hydroconversion rate (5). This MEL-type zeolite catalyst does not suffer from mass transport limitations, even under conditions where an equivalent MFI-type zeolite does (5) (Table 1). When comparing the two catalysts without mass transport limitations (5, 19), the MEL-type zeolite hydroisomerizes a higher percentage of the feed than the MFI-type zeolite catalyst (Table 1). Both the higher threshold for mass transport limitations and the higher hydroisomerization selectivity of the MEL-type zeolite indicate that branched C_{10} isomers have a lower chance for being converted when they are inside MEL-type pores than when they are inside MFI-type pores. This implies that the MEL-type zeolite either has an intrinsically lower consecutive-reaction rate or an intrinsically higher C_{10} diffusion rate than the MFI-type zeolite. So far there is no indication of a major difference in n-C_{10} or i-C_{10} diffusion rate between MEL- and MFI-type zeolites (13) suggesting that the difference must lie in the consecutive-reaction rate (5).

Primary hydrocracking product slates. Reconstruction of the primary hydrocracking product slates from the secondary hydrocracking product slates sheds some light on the different reactions that follow the formation of i-C_{10}. As discussed above, the composition of the C_5 fraction will be the same in both the primary and the secondary hydrocracking product slate, but all other product fractions require reconstruction. The effects of secondary ii-C_7 hydrocracking can be eliminated by adding one ii-C_7 molecule to the C_7 fraction for each set of one i-C_4 molecule and C_3 molecule removed from their respective product fractions until there are equal amounts of C_3 and C_7. This yields the primary C_3 fraction. The resultant C_4 fraction is representative for the primary C_4 fraction as well, for secondary hydroisomerization of C_4 is unlikely. The effects of secondary hydroisomerization on the resultant C_7 fraction can be eliminated, because the hydrocracking mechanism stipulates that the primary C_7 fraction consists 100% of i-C_7. Applying this procedure to the secondary hydrocracking product slate of the MEL-type zeolite (Fig. 2B) yields virtually complete primary i-C_4/n-C_6 and i-C_6/n-C_4 product pairs (Fig. 2D), indicating that the C_6 fraction has remained relatively unaffected by secondary reactions. Construction of a secondary hydrocracking product slate of the MFI-type zeolite based on the published data (19) (Fig. 2A) requires making the assumption that the composition of the carbon number fractions does not drastically change when the conversion is increased from 46 to 93% n-C_{10} conversion. If we apply our procedure to turn this secondary hydrocracking product slate into a primary one (Fig. 2C), the C_6 fraction contains 10% too much i-C_6 to complete the primary i-C_4/n-C_6 and i-C_6/n-C_4 product pairs. Therefore, i-C_6 and i-C_4 data are within the tabulated 15% error margin (Table 2).

Experimental ii-C_{10} selectivity. On the basis of the hydrocracking mechanism (39, 44, 45)(Figs. 3–5), it is possible to link the individual components of the primary C_{10} hydrocracking product slate (Table 2; Figs. 2C and 2D) to their ii-C_{10} precursors through four linear equations. Each 100 mol of ii-C_{10} consists of [n,m-DiMe-C_8] mol of n,m-dimethyl octane and hydrocrack into a known number of moles of branched isomers [i-C_x]. With these definitions in place, the individual hydrocracking reactions (Figs. 3 and 5) can be described as:

$$[2,2\text{-DiMe-C}_8] + u \cdot [2,4\text{-DiMe-C}_8] = [i\text{-C}_4] \quad [5]$$

$$[3,3\text{-DiMe-C}_8] + v \cdot [3,5\text{-DiMe-C}_8] = [i\text{-C}_5] \quad [6]$$

$$w \cdot [4,4\text{-DiMe-C}_8] + (1-v)[3,5\text{-DiMe-C}_8] = [i\text{-C}_6] \quad [7]$$

$$(1-w) \cdot [4,4\text{-DiMe-C}_8] + (1-u)[2,4\text{-DiMe-C}_8] = [i\text{-C}_7]. \quad [8]$$

In these equations u, v, and w are the probabilities that 2,4-, 3,5-, and 4,4-DiMe-C_8 split off either a small ($u, v, w > 0.5$) or a long ($u, v, w < 0.5$) iso-paraffin. Assuming that the ii-C_{10} precursors have no strong preference for splitting either way ($u \approx v \approx w \approx 0.5$) the solutions for the above four equations severely limit the possible ii-C_{10} hydrocracking precursors (Table 2).

In summary, a scrutiny of the published n-C_{10} hydroconversion data shows that of the two kinetically favored ii-C_{10} molecules (Fig. 4), the MFI-type zeolite predominantly

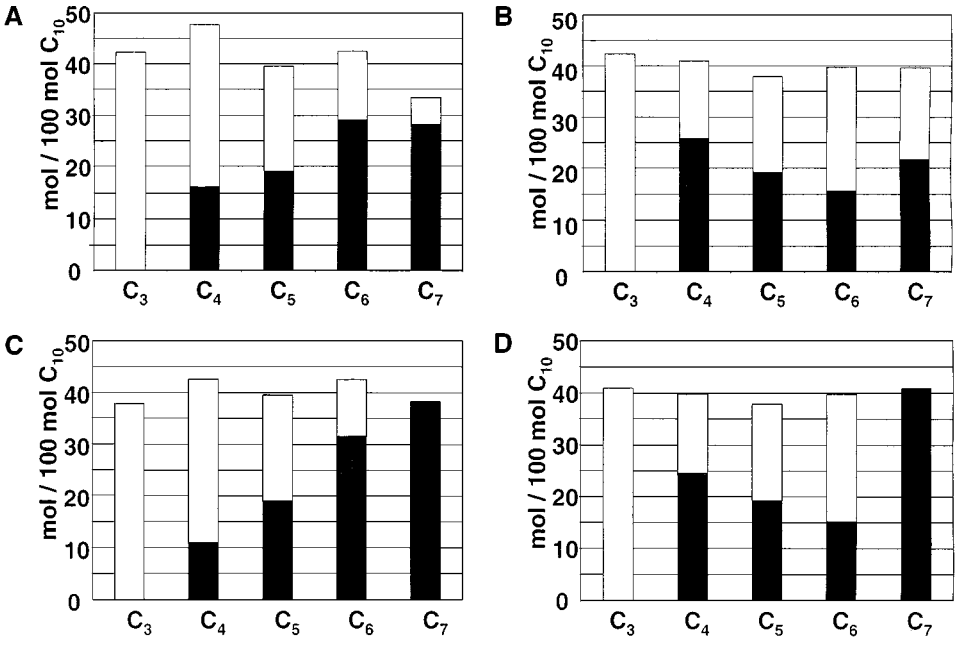

FIG. 2. The secondary (A and B) and primary (C and D) hydrocracking product slates of the MFI (A and C) and the MEL-type zeolites (B and D) at 46 and 49% *n*-C_{10} hydroconversion respectively (5, 19): normal (□) and branched (■) isomer yield.

hydrocracks the geminal *ii*-C_{10} (4,4-DiMe-C_8), whereas the MEL-type zeolite predominantly hydrocracks the quasi-vicinal *ii*-C_{10} (2,4-DiMeC_8) (Table 2). We can now turn to the free energies of formation as amenable by molecular simulations to see why there is such a marked difference in intrinsic shape selectivity.

TABLE 2

The Branched Primary Hydrocracking Products ([*i*-C_x] (mol/100 mol *n,m*-DiMe-C_8 Hydrocracked)) from the MFI- and MEL-Type Zeolites (4, 19) and Their Dimethyl Octane Precursors ([*n,m*-DiMe-C_8] (mol%) with Methyl Positions *n* and *m*) Assuming No Preferential Hydrocracking into Small or Large *i*-C_x

	MFI	MEL
Products		
[*i*-C_4]	15–11[a]	26
[*i*-C_5]	19	19
[*i*-C_6]	28–32[a]	16
[*i*-C_7]	38	40
Precursors		
[2,2-DiMe-C_8]	0–5[b]	0–2[b]
[3,3-DiMe-C_8]	14–19	17–19
[4,4-DiMe-C_8]	46–64	28–31
[2,4-DiMe-C_8]	30–12	52–48
[3,5-DiMe-C_8]	10–0	4–0

[a] The mass balance dictates that [*i*-C_7] + [*i*-C_6] + [*i*-C_5] + [*i*-C_4] = 100 mol/100 mol C_{10} hydrocracked.

[b] [*n,m*-DiMe-C_8] is in mol%, so that the individual values should add up to 100 mol%.

Simulated ii-C_{10} selectivity. The free energy of formation of the individual *ii*-C_{10} hydrocracking precursors inside the MFI- and MEL-type zeolites shed some light on the postulated differences in hydrocracking precursors. As indicated by a lower free energy of formation, MFI-type

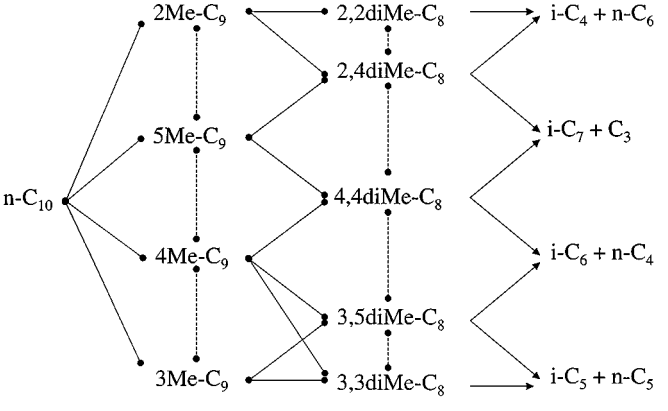

FIG. 3. Overview of the *n*-C_{10} hydroconversion (19, 39): equilibration between isomers with (●—●) or without (●- - -●) a change in the degree of branching and hydrocracking (→). Of all the *ii*-C_{10} isomers, only those with geminal or quasi-vicinal methyl groups are shown. The *ii*-C_{10} isomers with neither geminal nor quasi-vicinal methyl groups hydrocrack ~10^2 times more slowly than the isomers shown (46, 47). This leaves them ample time to hydroisomerize into *ii*-C_{10} isomers with geminal or quasi-vicinal methyl groups, for their hydroisomerization rate is ~10^3 times faster than their hydrocracking rate (46). Accordingly, the hydrocracking will be dominated by the *ii*-C_{10} isomers with geminal or quasi-vicinal methyl groups that are shown. Figures 4 and 5 elucidate the individual hydroisomerization and hydrocracking reactions.

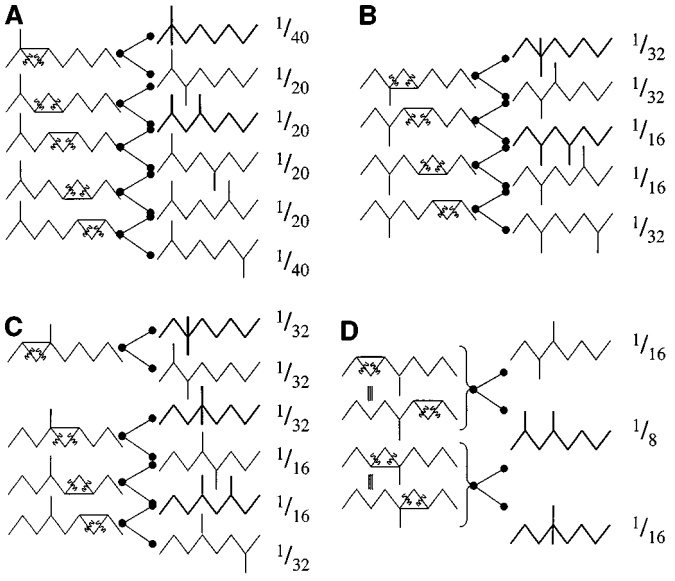

FIG. 4. The (protonated) cyclopropyl transition state (∇ and Δ) and the products for the hydroisomerization of *i*-C_{10} into *ii*-C_{10}. (A) 2-Me-C_9 hydroisomerization into **2,2-**, 2,3-, **2,4-**, 2,5-, 2,6-, 2,7-DiMe-C_8; (B) 3-Me-C_9 into **3,3-**, 3,4-, **3,5-**, 3,6-, 2,6-DiMe-C_8; (C) 4-Me-C_9 into **3,3-**, 2,3-, **4,4-**, 4,5-, **3,5-**, 2,5-DiMe-C_8; (D) 5-Me-C_9 into 3,4-, **2,4-**, **4,4-**DiMe-C_8 (39). Hydrocracking precursors are shown in bold. The probabilities of formation of the isomers are given, assuming no preferential formation for any *i*-C_{10} isomer or transition state. The shape selectivity imposed by the MEL- and MFI-type zeolites shifts the probability toward the *ii*-C_{10} and *i*-C_{10} isomers that have a shape commensurate with the MEL- and MFI-type pores (12). Of the paraffins with geminal methyl groups, 4,4-DiMe-C_8 has the highest chance of formation, of the paraffins with quasi-vicinal methyl groups, 2,4-DiMe-C_8 is favored. The probability of 4,4- and 2,4-DiMe-C_8 formation is further increased, because 5-Me-C_9 appears to be the *i*-C_{10} isomer preferentially retained (13, 32) and formed (Fig. 7; Table 5) by both MEL- and MFI-type zeolites.

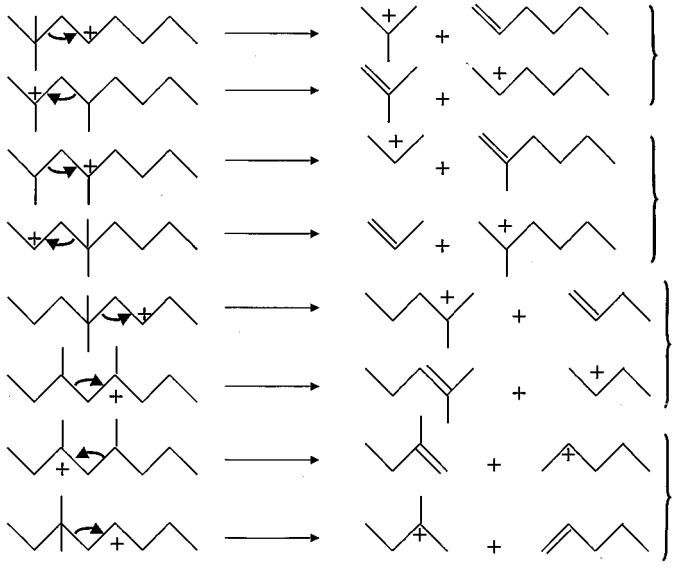

FIG. 5. Transitions states and intermediates for the hydrocracking of *ii*-C_{10} isomers with geminal or quasi-vicinal methyl groups (19). As all carbo-cationic and olefinic intermediates leave the catalysts as paraffins, carbo-cations and olefins with the same carbon backbone will end up as identical products, and are grouped together as such.

zeolites preferentially form geminal *ii*-C_{10}, whereas MEL-type zeolites preferentially form quasi-vicinal *ii*-C_{10} (Table 3). The reason for this selective decrease in free energy (Table 3) is that the shape of the MFI-type intersection (Fig. 1A) is commensurate with that of geminal *ii*-C_{10}, whereas the shape of the larger MEL-type intersection (Fig. 1B) is commensurate with that of quasi-vicinal *ii*-C_{10} (Fig. 6). Thus, the intersections constitute a mold for the formation of particular hydrocracking precursors. Once formed, the hydrocracking precursors will be trapped at the intersections, for they diffuse too slowly (12, 31) to leave the pores intact. The preference of MFI-type zeolites for geminal instead of quasi-vicinal *ii*-C_{10} becomes more evident when the temperature is increased from 415 to 523 K. Thus, the decreased free energy of formation of geminal *ii*-C_{10} inside MFI-type zeolites and of quasi-vicinal *ii*-C_{10} inside MEL-type zeolites supports the empirical observation that there is an intrinsic difference in their

TABLE 3

Gas Phase Free Energy of Formation (ΔG^{f}_{gas} (kJ/mol), from Literature (54) Data), Free Energy of Adsorption (ΔG_{ads} (kJ/mol)), Adsorption Enthalpy (ΔH_{ads} (kJ/mol)), and Free Energy of Formation Inside a Zeolite (ΔG^{f}_{sieve} (kJ/mol)) for Decane Isomers in MFI- or MEL-Type Silicas at 415 K

C_{10} isomer	ΔG^{f}_{gas} (kJ/mol)	MFI ΔG_{ads} (kJ/mol)	MEL ΔG_{ads} (kJ/mol)	MFI ΔH_{ads} (kJ/mol)	MEL ΔH_{ads} (kJ/mol)	MFI ΔG^{f}_{sieve} (kJ/mol)	MEL ΔG^{f}_{sieve} (kJ/mol)
n-C_{10}	150	−54	−49	−113	−112	96	101
2-Me-C_9	147	−53	−47	−112	−108	94	99
5-Me-C_9	150	−53	−52	−115	−113	96	98
2,2-DiMe-C_8	145	−48	−38	−105	−100	98	107
3,3-DiMe-C_8	147	−46	−37	−102	−97	101	110
4,4-DiMe-C_8	147	−50	−39	−106	−99	97	108
2,4-DiMe-C_8	150	−42	−55	−114	−117	108	96
3,5-DiMe-C_8	147	−37	−52	−106	−114	111	96
3,3,5-TriMe-C_7	154	−20	−22	−76	−91	134	132

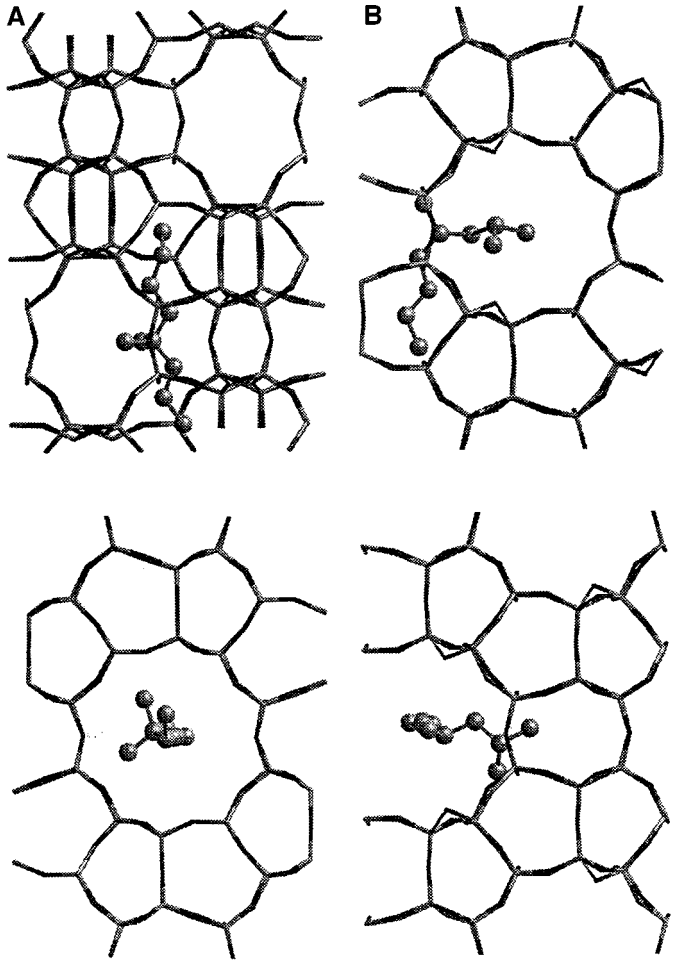

FIG. 6. Schematic drawing of the thermodynamically preferred positions of (A) 4,4-diMe-C_8 inside MFI-type zeolite, with octyl group in the straight channel and the methyl groups protruding into the sinusoidal channel, (B) 2,4-diMe-C_8 inside MEL-type zeolite, with a hexyl group in one straight channel and an iso-butyl group protruding into another straight channel. Paraffins are shown as ball-and-stick models, frameworks as sticks only. Top and bottom views are at a 90° angle from each other.

hydrocracking functionality and offers an explanation of why that is so.

Simulated ii-C_7 selectivity. The adsorption properties of *ii*-C_7 hydrocracking precursors (Table 4) are analogous to those of *ii*-C_{10} (Table 3). Again MFI-type zeolites lower the free energy of formation of *ii*-C_7 with geminal methyl groups and MEL-type zeolites lower that of the *ii*-C_7 with quasi-vicinal methyl groups (viz. 2,4-dimethyl pentane). Since *n*-C_{10} and *n*-C_7 hydroconversion are

TABLE 4

Gas Phase Free Energy of Formation (ΔG^{f}_{gas} (kJ/mol), from Literature Data (54)), Change of Free Energy of Formation by Zeolite (ΔG_{ads} (kJ/mol)), Adsorption Enthalpy (ΔH_{ads} (kJ/mol)), and Free Energy of Formation Inside a Zeolite (ΔG^{f}_{sieve} (kJ/mol)) for Heptane Isomers in MFI- or MEL-Type Silicas at 523 K

C_7 isomer	ΔG^{f}_{gas} (kJ/mol)	MFI ΔG_{ads} (kJ/mol)	MEL ΔG_{ads} (kJ/mol)	MFI ΔH_{ads} (kJ/mol)	MEL ΔH_{ads} (kJ/mol)	MFI ΔG^{f}_{sieve} (kJ/mol)	MEL ΔG^{f}_{sieve} (kJ/mol)
n-C_7	167	−27	−24	−78	−76	140	143
2-Me-C_6	164	−27	−25	−80	−79	137	140
3-Me-C_6	164	−26	−24	−78	−77	138	140
2,2-diMe-C_5	167	−24	−14	−74	−67	143	153
3,3-diMe-C_5	168	−18	−8	−68	−62	150	160
2,4-diMe-C_5	169	−13	−27	−73	−82	156	142
2,3-diMe-C_5	163	−25	−20	−78	−76	138	143

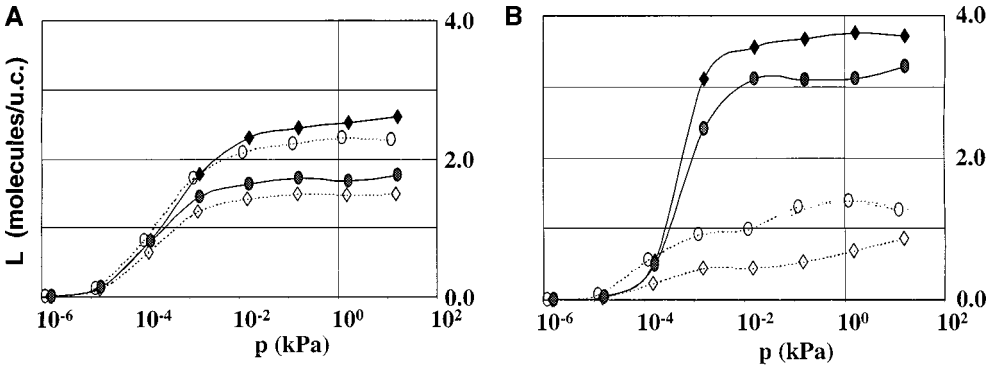

FIG. 7. The adsorption isotherm at 415 K as calculated by CBMC calculations of a binary mixture of 50% 2-methyl nonane (--◇--) and 50% *n*-decane (—◆—), and of 50% 5-methyl nonane (--○--) and 50% *n*-decane (—●—). (A) MFI-type and (B) MEL-type silica.

analogous, we would expect that MFI-type zeolites preferentially hydrocrack geminal *ii*-C_7, whereas MEL-type zeolites prefer the quasi-vicinal *ii*-C_7. Unfortunately this difference in the hydrocracking pathway is difficult to quantify, as the individual *ii*-C_7 precursors do not leave their signature in the C_7 hydrocracking product slate (Eq. [3]).

ii-C_{10} versus ii-C_7 hydrocracking. The difference in hydrocracking pathway between the MFI- and MEL-type zeolite can explain why an MFI-type zeolite hydrocracks a higher percentage of C_{10} feed but not of C_7 feed. Kinetic data show that at low temperatures (below 460–500 K for a C_8 feed) the geminal di-methyl paraffins preferred by the MFI-type zeolite have the highest hydrocracking rate, whereas at higher temperature (above 460–500 K for a C_8 feed) the quasi-vicinal di-methyl paraffins preferred by the MEL-type zeolite have the highest hydrocracking rate (47, 48). Since zeolites that hydrocrack paraffins at a higher rate will also hydrocrack a larger percentage of the feed, this can explain why MFI-type zeolites (at 400, 440, or 520 K) hydrocrack more C_{10} than MEL-type zeolites (at 430 K) (Table 1), but not more C_7 (all comparative tests at 523 K (8)). Although the low C_{10} and high C_7 hydroconversion test temperature can explain the low C_{10} and high C_7 hydrocracking selectivity of the MEL-type zeolite, it fails to explain why MEL-type zeolites reportedly have lower hydrocracking selectivity than MFI-type zeolites at temperatures as high as 655 K (6).

Simulated competitive adsorption. An alternative explanation for the differences in paraffin hydrocracking between MFI- and MEL-type zeolites follows from the dramatic selectivity difference that shows up in a study on the adsorption from mixtures of equal amounts of gaseous *n*-C_{10} and *i*-C_{10}. Both at low loading (Table 3) and at high loading (Fig. 7A), MFI-type zeolites adsorb *n*-C_{10} or *i*-C_{10} in approximately equal amounts, indicating that molecule–molecule interactions have only a minor effect on the free energy of adsorption (∼1 kJ/mol change) in MFI-type zeolites. In marked contrast, MEL-type zeolites develop a strong preference for linear paraffins at high loading (Fig. 7B). This preference corresponds to a decrease in the free energy of the adsorption (and of formation) of *n*-C_{10} relative to that of *i*-C_{10} of 4–5 kJ/mol (Table 5). A probable cause for the decrease in free energy of the linear paraffins relative to that of the branched paraffins is that the former can fill the pores with a higher packing efficiency (retaining a higher entropy) than the latter (cf. 24, 53). Closer inspection of the molecules shows that roughly half of the four MFI-type intersections per unit cell contain *i*-C_{10} molecules, whereas slightly fewer than half of the two large MEL-type intersections per unit cell still contain *i*-C_{10} at full loading. CBMC calculations indicate that full loading is obtained at 20 kPa C_{10} at temperatures up to 570 K and above 1 kPa C_{10} at temperatures near 415 K, i.e., at the *n*-C_{10} hydroconversion conditions discussed here (Table 1).

TABLE 5

Effect of Intermolecular Interactions on the Difference in the Free Energy of Adsorption between *i*-C_{10} and *n*-C_{10} ($\Delta G_{ads\,i} - \Delta G_{ads\,n}$ (kJ/mol))

i-C_{10} isomer	MFI empty $\Delta G_{ads\,i} - \Delta G_{ads\,n}$ (kJ/mol)	MFI full $\Delta G_{ads\,i} - \Delta G_{ads\,n}$ (kJ/mol)	MEL empty $\Delta G_{ads\,i} - \Delta G_{ads\,n}$ (kJ/mol)	MEL full $\Delta G_{ads\,i} - \Delta G_{ads\,n}$ (kJ/mol)
2-Me-C_9	0.8	1.8	1.7	5.7
5-Me-C_9	0.4	−0.9	−2.5	2.9

Note. We compare an "empty" zeolite (Henry regime, no intermolecular interactions, Table 3) with a "full" zeolite that is in equilibrium with a mixture consisting of equal amounts *n*-C_{10} and *i*-C_{10} at high loading (Fig. 7).

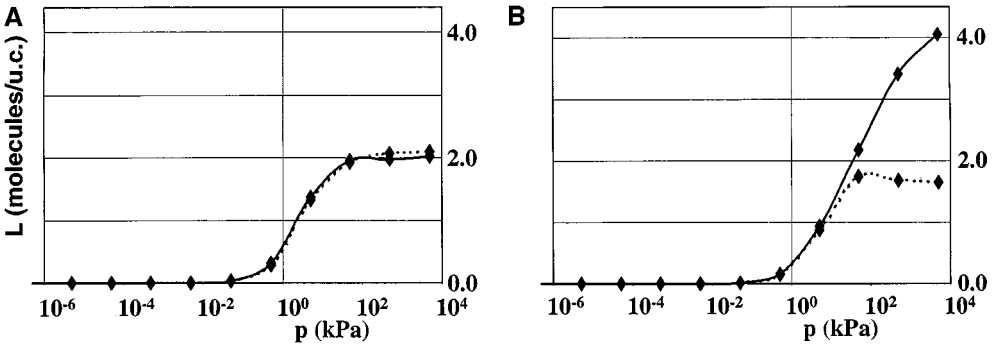

FIG. 8. The adsorption isotherm at 523 K as calculated by CBMC calculations of a binary mixture of 50% 2-methyl hexane (--◆--) and 50% *n*-heptane (—◆—). (A) MFI-type and (B) MEL-type silica.

Competitive adsorption in n-C_{10} hydroconversion. At full loading, molecule–molecule interactions impede formation of *i*-C_{10} out of *n*-C_{10} by increasing the free energy of formation of the former at the large MEL-type intersections. In addition, they impede hydroisomerization reactions following the formation of *i*-C_{10} by facilitating the (re-)adsorbtion of *n*-C_{10} at the cost of the (re-)adsorption of *i*-C_{10}. In MFI-type zeolites molecule–molecule interactions have no such marked effect (Tables 3 and 5). The formation of *ii*-C_{10} hydrocracking precursors from *i*-C_{10} by consecutive hydroisomerization reactions is further impeded by the limited availability of suitable sites in the MEL-type zeolites at full loading. There are only half as many large MEL-type intersections as there are MFI-type intersections (Fig. 1). Both the higher selectivity for absorbing linear instead of branched paraffins and the lower density of sites suitable for forming hydrocracking precursors will suppress consecutive hydrocracking reactions, and explain the lower hydrocracking selectivity (and higher hydroisomerization selectivity) of MEL-type zeolites.

No competitive adsorption in n-C_7 hydroconversion. Interestingly, the adsorption simulations not only explain why the MEL-type zeolite has a higher *n*-C_{10} hydroisomerization selectivity than the MFI-type zeolite, they also explain why this is not the case for the *n*-C_7 hydroisomerization (8) selectivity. The comparative *n*-C_7 hydroconversion tests where done at 10 kPa *n*-C_7, 523 K (8). At this temperature and pressure MFI- and MEL-type zeolites have a low enough loading (about one molecule per unit cell) for *n*-C_7 and *i*-C_7 to have a comparable free energy of formation in both MFI- and MEL-type zeolites (Fig. 8). In addition, there is no shortage of available sites at the intersections of these zeolites to form hydrocracking precursors. Thus, the *n*-C_7 hydroconversion tests were done at too low a C_7 loading for competitive adsorption of *n*-C_7 and *i*-C_7 to occur and so demonstrate the intrinsic selectivity differences between MFI- and MEL-type zeolites.

Actual hydrodewaxing tests. It is difficult to judge what the adsorption properties of MEL- and MFI-type zeolites are when a complex feedstock with paraffins significantly longer than C_{10} is converted at a temperature as high as 655 K (instead of the 430–523 K used for C_7 and C_{10}) (6). We are tempted to conclude that competitive adsorption between linear paraffins and branched paraffins will occur. In that case the lower density and lower accessibility of the large MEL-type intersections as compared to the MFI-type intersections will overrule the enhancement of the hydrocracking selectivity of MEL-type zeolite by the high operation temperature. To found such a conclusion more firmly would require more experimental studies quantifying the separate effects of temperature and loading on the paraffin hydroconversion selectivity of MEL- and MFI-type zeolites.

CONCLUSIONS

When the rate of the acid-catalyzed reactions determines the *n*-C_{10} hydroconversion rate, MFI- and MEL-type zeolites hydroisomerize normal paraffins into paraffins with geminal or quasi-vicinal methyl groups before they hydrocrack them. An analysis of the hydrocracking product slates and of the adsorption properties obtained by molecular simulations indicates that MFI-type zeolites intrinsically hydrocrack more geminal and fewer quasi-vicinal di-methyl paraffins than MEL-type zeolites. As geminal di-methyl paraffins hydrocrack faster than quasi-vicinal di-methyl paraffins at low temperature, but not at high temperature, the selectivity for geminal di-methyl paraffins explains why MFI-type zeolites hydrocrack more of a C_{10} feed than a MEL-type zeolite (selectivity tested at low temperature), but not more of a C_7 feed (tested at high temperature). The adsorption properties indicate that the higher selectivity of the MFI-type structure for adsorbing branched rather than linear paraffin reactants also contributes to its higher hydrocracking selectivity as compared to a MEL-type zeolite. As this higher reactant selectivity is only significant at sufficiently high loading, it also explains why MFI-type zeolites showed higher *n*-C_{10} hydrocracking (tested at high loading), but not higher *n*-C_7 hydrocracking

selectivity (tested at low loading) than a MEL-type zeolite.

ACKNOWLEDGMENTS

These investigations are supported in part by the Netherlands Research Counsil for Chemical Sciences (CW) with financial aid from the Netherlands Technology Foundation and by the Netherlands Organization for Scientific Research (NWO) through PIONIER. The authors wish to thank C. H. Roemkens, J. A. R. van Veen, W. H. J. Stork, A. L. Myers, H. Schenk, D. Frenkel, D. Dubbeldam, and M. S. Rigutto for their comments on our manuscript.

REFERENCES

1. Blauwhoff, P. M. M., Gosselink, J. W., Kieffer, E. P., Sie, S. T., and Stork, W. H. J., *in* "Catalysis and Zeolites" (J. Weitkamp and L. Puppe, Eds.), pp. 437–538. Springer, Berlin, 1999.
2. Chen, N. Y., Garwood, W. E., and Dwyer, F. G., "Shape Selective Catalysis in Industrial Applications," pp. 38–83. Dekker, New York, 1996.
3. Free, H. W. H., Schockaert, T., and Sonnemans, J. W. M., *Fuel Process. Technol.* **35**, 111–117 (1993).
4. Miller, S. J., *Microporous Mater.* **2**, 439–449 (1994).
5. Jacobs, P. A., Martens, J. A., Weitkamp, J., and Beyer, H. K., *Faraday Discuss. Chem. Soc.* **72**, 353–369 (1982).
6. Chen, N. Y., and Walsh, D. E., US patent 4,877,581 (1989).
7. Chester, A. W., Wilson, R. C., Oleck, S. M., and Yen, J. Hs-G., EP patent 0155822 (1985).
8. Giannetto, G., Perot, G., and Guisnet, M., *Stud. Surf. Sci. Catal.* **24**, 631–638 (1985).
9. Derouane, E.G., Dejaifve, P., Gabelica, Z., and Védrine, J. C., *Farad. Discuss. Chem. Soc.* **72**, 331–344 (1981).
10. Martens, J. A., and Jacobs, P. A., *Zeolites* **6**, 334–348 (1986).
11. (a) Meier, W. M., Olson, D. H., and Baerlocher, Ch., "Atlas of Zeolite Structure Types," 4th ed. Elsevier, London, 1996; (b) http://www.iza-structure.org/databases/ by Baerlocher, Ch., and McCusker L.B.
12. Schenk, M., Smit, B., Vlugt, T. J. H., and Maesen, Th. L. M., *Angew. Chemie Int. Ed. Engl.* **40**(4), 736–739 (2001).
13. Webb, E. B., III, and Grest, G. S., *Catal. Lett.* **56**, 95–104 (1998).
14. Raybaud, P., Patrigeon, A., and Toulhoat, H., *J. Catal.* **197**, 98–112 (2001).
15. Siepmann, J. I., and Frenkel, D., *Mol. Phys.* **75**, 59–70 (1992).
16. Frenkel, D., Mooij, G. C. A. M., and Smit, B., *J. Phys.: Condens. Matter.* **4**, 3053–3076 (1992).
17. De Pablo, J. J., Laso, M., and Suter, U. W., *J. Chem. Phys.* **967**, 6157–6162 (1992).
18. Guisnet, M., Alvarez, F., Giannetto, G., and Perot, G., *Catal. Today* **1**, 415–433 (1987).
19. Weitkamp, J., Jacobs, P. A., and Martens, J. A., *Appl. Catal.* **8**, 123–141 (1983).
20. Jacobs, P. A., Uytterhoeven, J. B., Steyns, M., Froment, G., and Weitkamp, *in* "Proceedings of the Fifth International Conference on Zeolites" (L. V. C. Rees, Ed.), pp. 607–615. Heyden, London, 1980.
21. Martens, J. A., Tielen, M., and Jacobs, P. A., *Acta Chim. Hung.* **119**, 203–212 (1985).
22. Martens, J. A., Parton, R., Uytterhoeven, L., Jacobs, P. A., and Froment, G. F., *Appl. Catal.* **76**, 95–116 (1991).
23. Jacobs, P. A., Derouane, E. G., and Weitkamp, J., *J. Chem. Soc. Chem. Commun.* **12**, 591–593 (1981).
24. Vlugt, T. J. H., Krishna, R., and Smit, B., *J. Phys. Chem. B* **103**, 1102–1118 (1999).
25. Bezus, AG, Kiselev, A. V., Lopatkin, A. A., and Du, P. Q., *J. Chem. Soc. Faraday Trans. II* **74**, 367–379 (1978).
26. June, R. L., Bell, A. T., and Theodorou, D. N., *J. Phys. Chem.* **96**, 1051–1060 (1992).
27. Smit, B., and Siepmann, J. I., *J. Phys. Chem.* **98**, 8442–8452 (1994).
28. Maesen, Th. L. M., Schenk, M., Vlugt, T. J. H., De Jonge, J. P., and Smit, B., *J. Catal.* **188**, 403–412 (1999).
29. June, R. L., Bell, A. T., and Theodorou, D. N., *J. Phys. Chem.* **94**, 1508–1516 (1990).
30. Giannetto, G. E., Perot, G. R., and Guisnet, M. R., *Stud. Surf. Sci. Catal.* **20**, 265–272 (1984).
31. Smit, B., Loyens, L. D. J. C., and Verbist, G. L. M. M., *Faraday Discuss.* **106**, 93–104 (1997).
32. Webb, E. B., III, Grest, G. S., and Mondello, M., *J. Phys. Chem. B* **103**, 4949–4959 (1999).
33. Haag, W. O., Lago, R. M., and Weisz, P. B., *Faraday Discuss. Chem. Soc.* **72**, 317–330 (1982).
34. Post, M. F. M., Van Amstel, J., and Kouwenhoven, H. W., *in* "Proceedings, 6th International Zeolite Conference" (D. H. Olson and A. Bisio, Eds.), pp. 517–527. Butterworths, Guildford, 1983.
35. Voogd, P., and Van Bekkum, H., *Stud. Surf. Sci. Catal.* **65**, 467–478 (1990).
36. Namba, S., Sato, K., Fujita, K., Kim, J. H., and Yashima, T., *Stud. Surf. Sci. Catal.* **28**, 661–668 (1986).
37. Giannetto, G. E., Perot, G. R., and Guisnet, M. R., *Ind. Eng. Chem. Prod. Res. Dev.* **25**, 481–490 (1986).
38. Lugstein, A., Jentys, A., and Vinek, H., *Appl. Catal.* **166**, 29–38 (1998).
39. Martens, J. A., and Jacobs, P. A., *in* "Theoretical Aspects of heterogeneous Catalysis" (J. B. Moffat, Ed.), pp. 52–109. Van Nostrand Reinhold, New York, 1990.
40. Höchtl, M., Jentys, A., and Vinek, H., *J. Catal.* **190**, 419–432 (2000).
41. Weisz, P. B., *Adv. Catal.* **13**, 137–190 (1962).
42. Coonradt, H. L., and Garwood, W. E., *Ind. Eng. Chem., Prod. Res. Dev.* **3**, 38–45 (1964).
43. Degnan, T. F., and Kennedy, C. R., *AIChE J.* **39**(4), 607–614 (1993).
44. Martens, J. A., Jacobs, P. A., and Weitkamp, J., *Appl. Catal.* **20**, 283–303 (1986).
45. Martens, J. A., Tielen, M., and Jacobs, P. A., *Catal. Today* **1**, 435–453 (1987).
46. Alvarez, F, Ribeiro, F. R., Perot, G., Thomazeau, C., and Guisnet, M., *J. Catal.* **162**, 179–189 (1996).
47. (a) Svoboda, G. D., Vynckier, E., Debrabandere, B., and Froment, G. F., *Ind. Eng. Chem. Res.* **34**, 3793–3800 (1995); (b) Martens, G., and Froment, G. F., *Stud. Surf. Sci. Catal.* **122**, 333–340 (1999).
48. Martens, G. G., Marin, G. B., Martens, J. A., Jacobs, P. A., and Baron, G. V., *J. Catal.* **195**, 253–267 (2000).
49. Kondo, J. N., Ishikawa, H., Yoda, E., Wakabayashi, F., and Domen, K., *J. Phys. Chem. B* **103**, 8538–8543 (1999).
50. Froment, G. F., *Catal. Today.* **1**, 455–473 (1987).
51. Weitkamp, J., *in* "Hydrocracking and Hydrotreating," ACS Symposium Series, Vol. 20, pp. 1–27. Am. Chem. Soc., Washington, DC, 1975.
52. DeNayer, J. F., Bouyermaouen, A., and Baron, G. V., *Ind. Eng. Chem. Res.* **37**, 3691–3698 (1998).
53. Krishna, R., Smit. B., and Vlugt, T. J. H., *J. Phys. Chem. A.* **102**, 7727–7730 (1998).
54. Stull, D. R., Westrum, E. F., Jr., Sinke G. C., "The Chemical Thermodynamics of Organic Compounds," pp. 249–252, 276–284. Krieger, Malabar, FL, 1987.